Chemical Engineering Journal 187 (2012) 334–340

Contents lists available at SciVerse ScienceDirect

Chemical Engineering Journal

journal homepage: www.elsevier.com/locate/cej

Tunable electrical conductivity and dielectric properties of triglycine sulfate-polypyrrole composite

Saswata Bose[a], Ananta Kumar Mishra[b], Tapas Kuila[a], Nam Hoon Kim[c], Ok-Kyung Park[a], Joong Hee Lee[a,b,*]

[a] WCU Program, Department of BIN Fusion Technology, Chonbuk National University, Jeonju, Jeonbuk, 561-756, Republic of Korea
[b] Department of Polymer and Nano Engineering, Chonbuk National University, Jeonju, Jeonbuk, 561-756, Republic of Korea
[c] Department of Hydrogen and Fuel Cell Engineering, Chonbuk National University, Jeonju, Jeonbuk, 561-756, Republic of Korea

ARTICLE INFO

Article history:
Received 29 September 2011
Received in revised form 9 January 2012
Accepted 17 January 2012

Keywords:
Triglycine sulfate
Polypyrrole
Ferroelectric
Conductivity
Dielectric permittivity

ABSTRACT

Triglycine sulfate (TGS) crystals were grown from aqueous solution using a slow evaporation technique. Polypyrrole (PPy)/TGS composites were prepared by ex situ technique employing solvent casting method. TGS crystal showed a second-order phase transition at 49 °C, which confirms its ferroelectric nature. The XRD pattern of PPy/TGS composites showed the effective filler-polymer matrix interaction. The morphologies of the composites were analyzed through field emission transmission electron microscopy. A gradual increment in DC conductivity of PPy was observed with increase in temperature, revealing its semi-conducting behavior. PPy/TGS composites also demonstrated a similar trend but with drastic decrement in conductivity value, highlighting the insulating behavior of TGS. The dielectric loss of the composites was significantly lower compared to PPy. Despite low dielectric permittivity, PPy/TGS composite can be effectively utilized as memory devices due to its low dielectric loss.

1. Introduction

Triglycine sulfate (TGS) is an important ferroelectric material for technological applications including infrared detectors and pyroelectric vidicon tubes [1–3]. TGS crystal shows a typical second-order ferroelectric phase transition at the Curie point (~49 °C). Below the Curie point, TGS possesses a polar point group in the monoclinic system; above the Curie point, TGS has a non-polar point group in the monoclinic system [1,4–6]. Curie temperature is the temperature below which the TGS crystals are ferroelectric and above which the crystals show paraelectric behavior. To develop a memory device, the material should possess relatively high dielectric permittivity with minimum dielectric loss. Ferroelectric materials, such as TGS, contribute towards the high pyroelectric activity with relatively low dielectric permittivity [5,7]. Alternatively, conducting polymer with substantially high dielectric permittivity gives rise to the loss factor of the material. Therefore, conducting polymer-ferroelectric ceramic composite material may be useful from the perspective of achieving memory devices with low dielectric loss. Conducting polymers shows very high dielectric permittivity owing to their high electrical conductivity which causes a considerable increment in the loss factor. TGS is an insulating material which in turn attributes to low dielectric permittivity. Incorporation of TGS can effectively reduce the dielectric loss of the material, which is the prime requirement in memory device application.

Venkatragavaraj et al. [8] studied the piezoelectric properties of ferroelectric PZT-poly(vinylidene fluoride) (PVDF) composites. The samples were prepared using solvent casting method as well as hot-press technique. The solvent casting method requires a substantial improvement to ensure better homogeneity and avoid porosity. The piezoelectric strain coefficient (d_{33}) of the composite was determined to be 13.8 pCN^{-1} employing hot-press technique.

Recently, dielectric properties of PVDF-based nanocomposites filled with surface hydroxylated $BaTiO_3$ nanoparticles were reported by Zhou et al. [9]. The dielectric properties of the nanocomposite based upon hydroxylated $BaTiO_3$ showed weaker frequency dependency as compared to that of crude $BaTiO_3$-based nanocomposite. On the other hand, hydroxylated $BaTiO_3$- based nanocomposite exhibited lower loss tangent and higher dielectric strength.

Yang et al. [10] demonstrated the pyroelectric properties of triglycine sulfate/poly(vinylidene fluoride-trifluoroethylene) composites. Three kinds of composite samples e.g., unpoled composites, composites with only the TGS phase poled and composites with

* Corresponding author at: WCU Program, Department of BIN Fusion Technology, Chonbuk National University, Jeonju, Jeonbuk, 561-756, Republic of Korea.
Tel.: +82 63 270 2342; fax: +82 63 270 2341.
E-mail address: jhl@jbnu.ac.kr (J.H. Lee).

1385-8947/$ – see front matter © 2012 Elsevier B.V. All rights reserved.
doi:10.1016/j.cej.2012.01.081

both phases poled were prepared using solvent casting method followed by compression molding. The relative permittivity of these composites was in line with the predictions of the Bruggeman model. When the TGS and copolymer phases were poled in the same direction, the piezoelectric activities of the two phases partially canceled each other while strengthening of pyroelectric activities was evident.

Dielectric properties of ferroelectric barium titanate-acrylic resin composites were investigated by Robertson and Hall [11]. The dielectric characteristics of composites prepared using fine and coarse grades of barium titanate powders are compared. The composites of fine-grained barium titanate powders with polymer exhibited a typical Rayleigh coefficient of $3 \times 10^{-6}\,mV^{-1}$. On the other hand composites of coarse-grained barium titanate powders with polymer displayed significantly higher Rayleigh coefficients, up to $7 \times 10^{-6}\,mV^{-1}$. The saturation in the dielectric behavior of the composites with coarse-grained barium titanate powders was explained in terms of particle size effects and the development of an improved flux path through the ferroelectric particles by particle–particle contacts.

Pant et al. [12] revealed the dielectric properties of composites of $BaTiO_3$ with polyaniline and maleic resin. Dielectric constant of the composites of $BaTiO_3$ with maleic resin followed the asymmetric Bruggeman model, the normal way. On the other hand the composites of $BaTiO_3$ with polyaniline showed unfamiliar behavior. Even at a low concentration of polyaniline (5 wt%) there was a marked reduction in the dielectric constant of $BaTiO_3$ indicated towards the coating of $BaTiO_3$ particles by PANI which in turn was attributed to the highly surface adsorbing character.

In the current study, polypyrrole (PPy) has been chosen as the conducting polymer matrix owing to its high electrical conductivity accompanied with high stability when exposed to ambient conditions, ease of synthesis, and cost effectiveness [13–17]. TGS, a well-known ferroelectric material, shows a low relative permittivity, would be an ideal material to be used as the inclusion phase with PPy. The aim of our study is to develop novel TGS/PPy composite as a potential material for memory device application.

2. Experimentation

2.1. Materials used

Glycine, ammonium persulfate (APS) and pyrrole were purchased from Sigma–Aldrich, USA. Sulfuric acid was purchased from Samchun Pure Chemical Co. Ltd., South Korea. Dodecyl benzene sulfonic acid (DBSA) was purchased from Tokyo Chemical Industry Company Ltd., Japan.

2.2. Synthesis and growth of TGS crystal

AR grade glycine and concentrated sulfuric acid were dissolved in de-ionized water (3:1 molar ratio) to obtain the synthesized salt solution of TGS. Temperature of the reaction mixture was maintained at 50 °C to avoid salt decomposition. Purity of the synthesized salt was achieved by successive recrystallization. Growth of the TGS crystals was conducted by slow evaporation technique at room temperature. The recrystallized TGS salt was utilized to prepare saturated salt solution and then the solution was filtered using Whatmann 41 filter paper (pore size ~ 20 μm). Subsequently, the filtered solutions were stored in a beaker covered with porous papers. Large-sized crystals with good quality were grown after 30 days. The associated chemical reaction for the TGS crystal formation is shown below.

$$NH_2CH_2COOH + H_2SO_4 \rightarrow (NH_2CH_2COOH)_3H_2SO_4$$

2.3. Synthesis of PPy–DBSA complex

Aqueous DBSA solution (0.075 mol) was added to pyrrole monomer (0.149 mol) in distilled water and stirred vigorously for 30 min. Subsequently, aqueous ammonium persulfate solution (0.016 mol) was slowly added. The reaction was allowed to continue for 24 h at room temperature with continuous stirring. During the polymerization process, the color of the solution changed from brown to black. The polymerization reaction was terminated with the addition of excess methanol. The black powdery polymer was washed several times with water and methanol and dried under vacuum at 60 °C for 24 h.

2.4. Fabrication of TGS/PPy–DBSA composite

PPy–DBSA powder was dissolved in N,N-dimethyl formamide (DMF) solution by ultrasonication for 30 min. TGS powder (obtained via ball milling) was dispersed into the solution of PPy and DMF by ultrasonication for another 30 min. The resulting solution was stirred at 60 °C for 24 h, and the prepared composites were dried under vacuum at 80 °C for 24 h. TGS/PPy–DBSA composites loaded with 5, 10, 25, and 50 wt% of TGS were designated

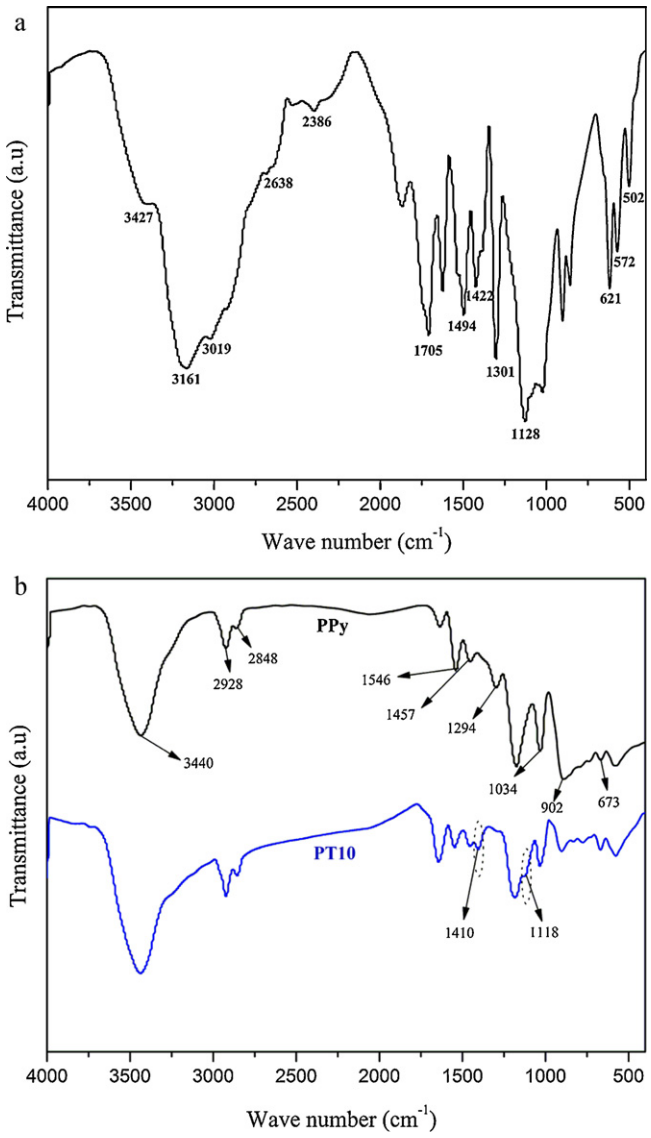

Fig. 1. FTIR spectroscopy of (a) TGS and (b) PPy and PT10.

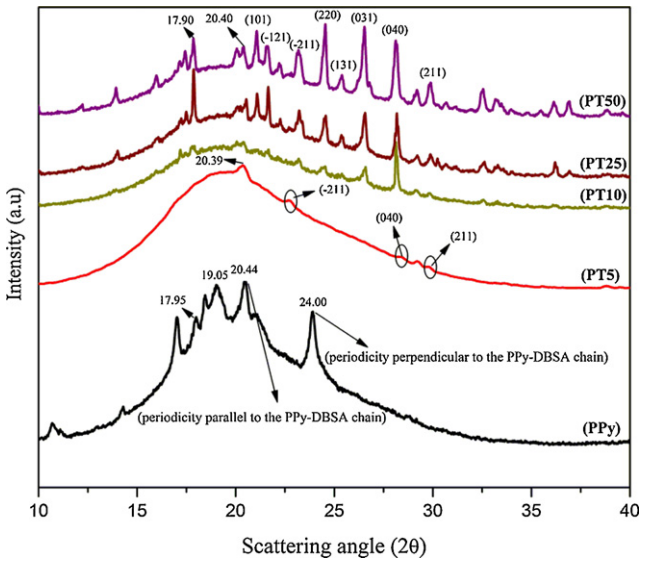

Fig. 2. XRD pattern of PPy, PT5, PT10, PT25, and PT50.

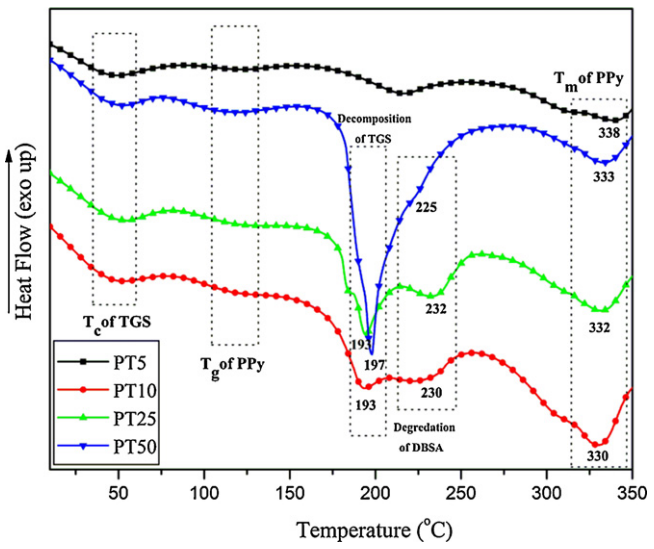

Fig. 4. DSC of PT5, PT10, PT25, and PT50.

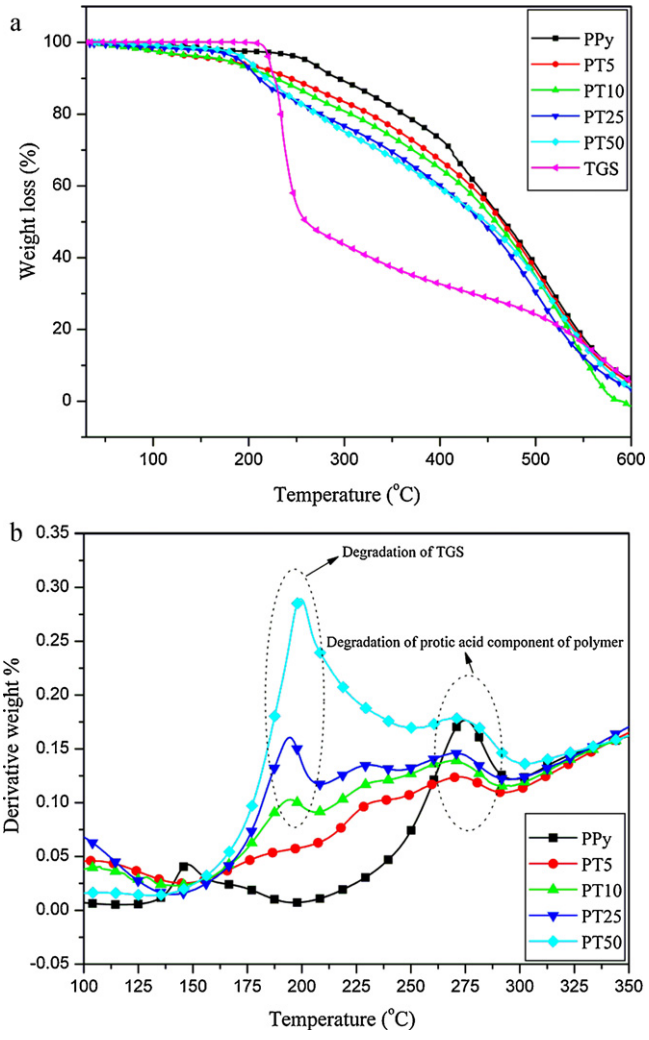

Fig. 3. (a) TGA of PPy, TGS, and their composites and (b) DTG of PPy and its composites with TGS at different weight ratios.

as PT5, PT10, PT25, and PT50, respectively and PPy–DBSA complex was designated as PPy.

3. Characterization

Fourier transformed infrared spectroscopy (FTIR) study of the materials was conducted using a Nicolet 6700 spectrometer (Thermo Scientific, USA) at room temperature over a frequency range of 4000–500 cm^{-1}. The crystallographic structures of the materials were determined via X-ray diffraction (XRD). The XRD analysis was performed using a D/Max 2500 V/PC diffractometer (Rigaku Corporation, Japan) with Cu-Kα targets (λ = 0.154 nm) at a scanning rate of 0.020 2θ/s, chart speed of 10 mm/2θ, and operated at a voltage of 40 kV and current of 100 mA. Thermogravimetric analysis (TGA) was conducted under air using Q50 TGA (TA Instruments, USA) in the temperature range of 30–600 °C, with a heating rate of 5 °C/min. Differential scanning calorimetry (DSC) analysis of TGS and the composite was performed using Q-20 (TA Instruments, USA) in the temperature range of −10–120 °C and −10–350 °C, respectively with a heating rate of 3 °C/min. Field emission scanning electron microscopy (FESEM) observations were carried out in a JSM-6701F (JEOL, Japan). The powder samples were placed on an aluminum holder and then coated with a thin layer of platinum. Electrical resistivity of the materials was measured by two-probe method. Powdery samples were pressed into disk pellets with a diameter of 12.5 mm and the average thickness of about 1 mm. Dielectric measurements of the pellets were performed using LCR meter (Agilent 4284A, Japan).

Table 1
Variation of weight losses at different temperature.

Sample	Weight loss (%) at different temperature				
	150 °C	250 °C	300 °C	400 °C	500 °C
PPy	1.7	4.1	10.9	27.0	62.8
PT5	3.6	10.8	16.9	33.1	64.2
PT10	3.6	12.7	19.2	35.5	65.7
PT25	2.2	16.2	23.5	40.0	69.7
PT50	1.8	16.5	24.8	40.7	65.8
TGS	–	45.0	56.4	67.0	76.1

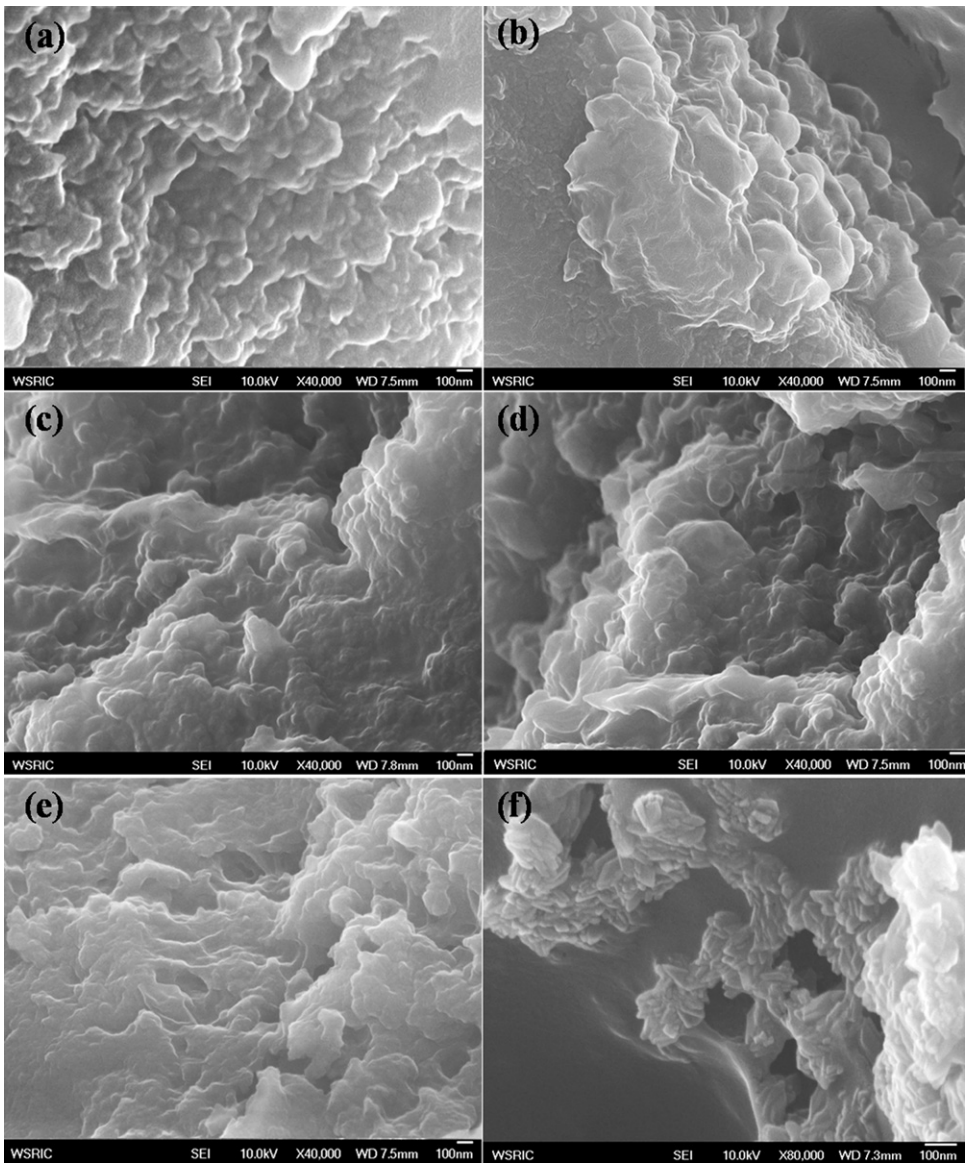

Fig. 5. FESEM image of (a) PPy, (b–e) PPy/TGS composites with 5, 10, 25, and 50 wt% of TGS, respectively, and (f) distribution of TGS throughout the matrix.

4. Results and discussion

FTIR spectroscopy of pure TGS is shown in Fig. 1a. TGS demonstrated a broad band in the region of 3427–2386 cm^{-1} which was due to combination of O—H and N—H stretching. The C—H and N—H bending vibrations appeared at 1494 and 1422 cm^{-1}, respectively. The respective bands at 1705 and 1128 cm^{-1} were due to C=O and C—O stretching vibrations. The strong band at 1301 cm^{-1} was due to asymmetric stretching vibration of S=O. Torsional oscillation of amine group of TGS appeared at 621, 572, and 502 cm^{-1} [5]. FTIR spectroscopy of PPy and PT10 are shown in Fig. 1b. FTIR spectrum of PPy showed a band at 3440 cm^{-1} attributing to N—H stretching vibration. The peaks at 2928 and 2848 cm^{-1} were designated as the asymmetric stretching and symmetric vibrations of C—H group [15]. The bands at 1546 and 1457 cm^{-1} corresponded to C—C and C—N stretching vibrations, respectively. The bands at 1294 and 1034 cm^{-1} were assigned to C—N and C—H in plane deformation vibrations, respectively. The bands at 902 and 673 cm^{-1} were due to C—H and C—C out of plane ring deformation [17]. However, FTIR spectrum of PT10 revealed two additional bands, one at 1410 cm^{-1} and other at 1118 cm^{-1}, indicating the presence of TGS in the composite.

Fig. 2 presents the XRD pattern of PPy and its composite at different TGS weight ratios. PPy showed some degree of semi crystalline nature. A broad band in the region of $2\theta = 10–30^{\circ}$ was observed for PPy, along with four distinguishable peaks at angles of 17.95°, 19.05°, 20.44°, and 24.00°. The peaks at 20.44° and 24.00° were ascribed to the periodicities parallel and perpendicular to the PPy chain, respectively [18–20]. However, incorporation of TGS crystal in the polymer matrix results in significant changes in the crystalline behavior of the material. With increasing TGS-loading, strong crystalline peaks of TGS were evident in the composites and the crystallinity offered by DBSA in PPy matrix was slightly hampered. Basically at higher TGS- loading, the crystalline peaks were more intense, suggesting contribution of highly crystalline TGS.

Fig. 3a shows the thermal stability of TGS, PPy and their composites. The decomposition temperature of TGS was observed at 214 °C. On the other hand, PPy showed a three-step degradation process. Initial weight loss in PPy was perhaps due to the volatilization of water molecules and oligomers as well as unreacted monomer

elimination. The second weight loss was due to decomposition of DBSA, i.e., the protonic acid component from the PPy matrix [18]. Finally at higher temperature the weight loss was due to degradation of polymer backbone resulting in the production of volatile gases [21,22]. However, the thermal stability of the composite materials was comparable to PPy at lower temperature, but lowered at higher temperature range (250–400 °C), ascribing to the reduced thermal stability of TGS above 200 °C. The subsequent weight losses of the concerned materials were also confirmed from the DTG curve (Fig. 3b). Variation of weight losses at different temperature is summarized in Table 1.

Fig. 4 shows the DSC of the PPy/TGS composites. An endothermic dip at 117 °C corroborated to the glass transition temperature (T_g) of polypyrrole [23]. Incorporation of TGS did not have significant effect on the T_g and melting temperature (T_m) of PPy. Appearance of broad endothermic peak in the region of 330–338 °C suggested the melting temperature of PPy. Upon increasing the TGS loading, the endothermic peak, due to degradation of DBSA from PPy backbone chain, shifted from 230 °C (at 10 wt% TGS loading) to 225 °C (at 50 wt% TGS loading). A sharp endothermic peak in the region of 193–197 °C was attributed to the decomposition of TGS.

The effect of TGS on the morphology of PPy was investigated by FESEM. Fig. 5a shows the morphology of PPy. Morphologies of the composites with 5, 10, 25, and 50 wt% TGS, are shown in Fig. 5b–e, respectively. A typical nano-spherical structure with a uniform size distribution was evident for PPy (Fig. 5a). The distribution of spherically shaped PPy was also evident in the composites (Fig. 5b–e); however, the composite surfaces appeared to be rougher than pure PPy, indicating the presence of TGS. Arrangement of TGS throughout the matrix is shown in Fig. 5f.

The effect of DBSA concentration on the electrical conductivity of PPy powder is shown in Fig. 6a. The electrical conductivity of PPy increased with DBSA concentration and saturated at the DBSA concentration of 0.30 mol. DBSA acted as the counterions with PPy polycations and thus resulted in gradual enhancement of electrical conductivity of PPy. Fig. 6b shows a logarithmic plot of electrical conductivity versus temperature for PPy and its composites with TGS. The conductivity of PPy was enhanced with increasing temperature, corroborating the excitation of electrons from the valance band to the conduction band and thus revealing the semiconducting behavior of PPy. Protonic acid (DBSA) had also a positive influence towards the enhancement in conductivity of PPy with temperature, which was caused by the mobility of counter-ions at higher temperature. However, the conductivity of the composites was also found to follow the similar trend as observed in PPy; conductivity increased with increasing temperature, but with a drastic reduction in the conductivity compared to that of pure PPy. The decrement in the conductivity can be ascribed to surface effect of TGS. The surface layers of TGS crystals cannot be considered as stable lattice and in fact are quite amorphous, which may have an influence on the motion of charge carriers leading to reduction in conductivity [21]. Fig. 6c shows the temperature-dependent conductivity of PPy and the PPy/TGS composites as a function of TGS loading. With increasing the amount of TGS, the conductivity was found to decrease. The conductivity at room temperature was lower than that observed in higher temperature irrespective of loading.

Size of TGS is supposed to play an imposing role towards the dielectric properties of TGS and its composites with PPy. Dielectric permittivity (ε') of TGS at 100 KHz as a function of TGS-size is shown in Fig. 7a. Dielectric permittivity (ε') of TGS was increased with an increase in size of TGS particles. In this study, PPy/TGS composites at different TGS loadings with TGS-size varying in the range of 350–450 μm, were considered for dielectric measurements. The ε' value of TGS in that range was 45–50. The dispersion of larger-sized TGS particles in PPy matrix had been an issue of major concern and alternatively, lower-sized TGS particles showed very low ε' value. Henceforth, TGS particles of intermediate size (350–450 μm) with a reasonably high ε' value were chosen for further studies.

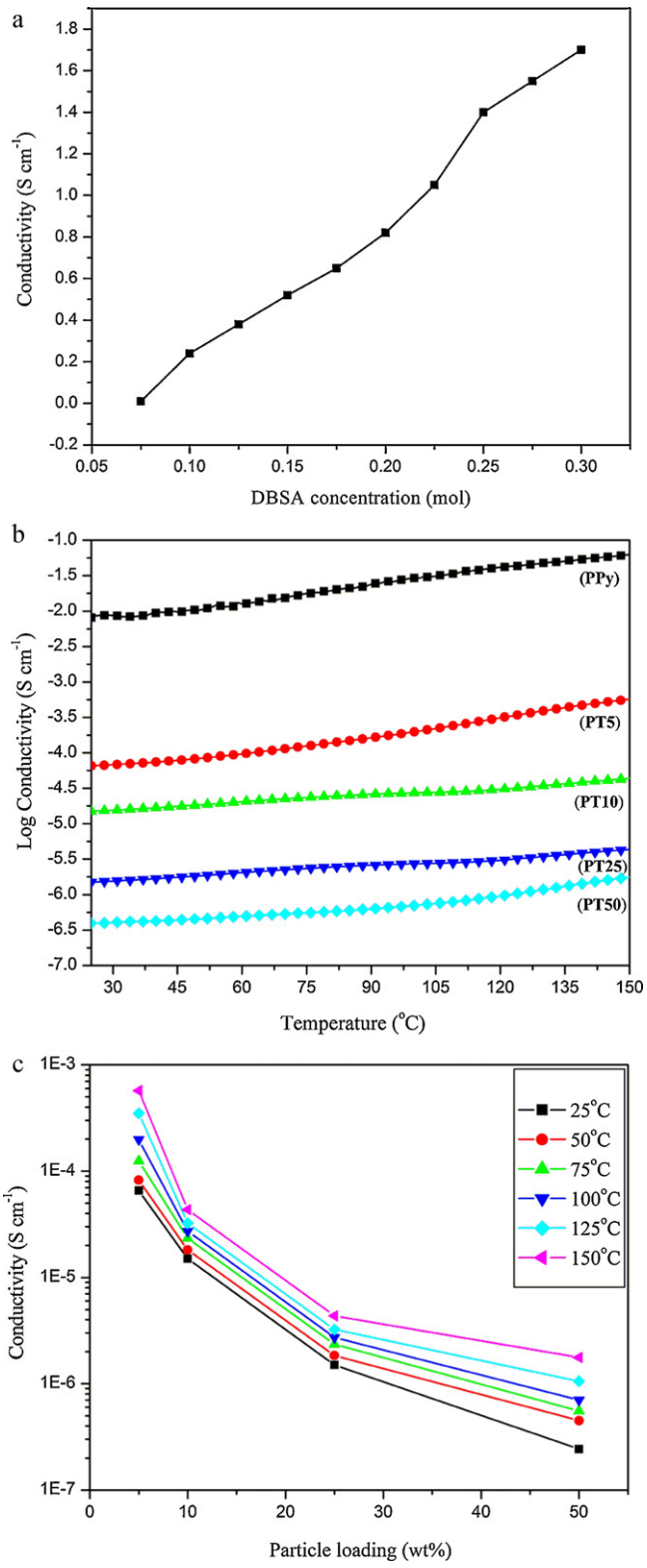

Fig. 6. (a) Effect of DBSA concentration of the DC conductivity of PPy, (b) variation of DC conductivity as a function of temperature for PPy and PPy/TGS composites, (c) temperature-dependent conductivity of PPy and the PPy/TGS composites as a function of TGS-loading.

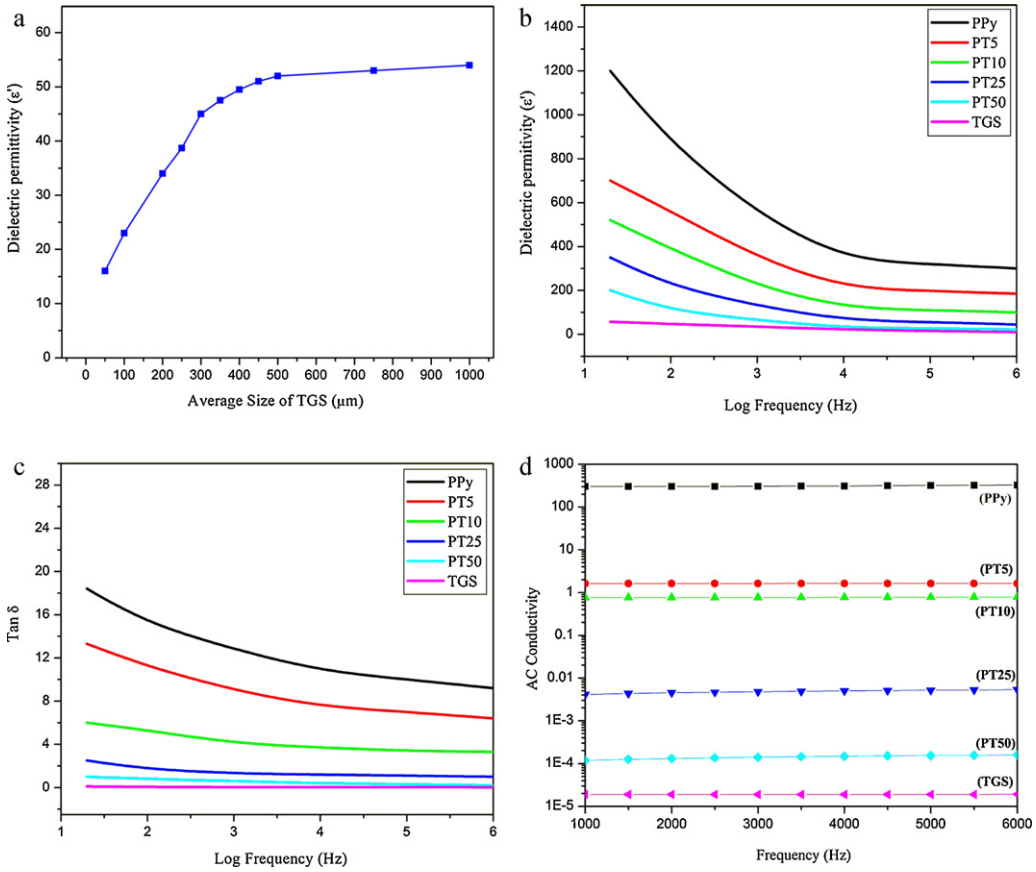

Fig. 7. (a) Evaluation of dielectric permittivity (ε') as a function of size of TGS powder at 100 KHz, (b) variation in dielectric permittivity (ε') as a function of frequency for PPy and its composites with different loading of TGS at room temperature, (c) variation of loss factor ($\tan\delta$) with frequency for PPy and PPy/TGS composites, and (d) variation in AC conductivity of PPy and PPy/TGS composites as a function of frequency.

Fig. 7b shows the variation in dielectric permittivity (ε') as a function of frequency for PPy and its composites with different loading of TGS at room temperature. The ε' of PPy was very high probably due to the highly conducting behavior of PPy. Incorporation of TGS had a significant effect towards the variation of ε' of the materials. Dielectric permittivity ε' of the composite materials is significantly lower compared to that of PPy, corroborating the dilution effect of TGS. The interesting observation was that the ε' values of PPy and its corresponding composites with TGS were decreased with an increment in frequency from 20 Hz to 1 MHz. However, the decrement in ε' for the composites was much slower compared to PPy suggesting improved frequency stability of the composites. On the other hand, high ε' values at low frequency region as compared to high frequency region for all the samples were due to interfacial polarization i.e., accumulation of bound charges at the interfaces of the bulk samples [24].

The variation of loss factor ($\tan\delta$) with frequency for PPy and PPy/TGS composites is shown in Fig. 7c. It had been observed that the dielectric loss factor decreased with increasing frequency. Moreover, decrement in loss tangent was more pronounced in low frequency region, probably due to mobile charges within the polymer backbone. The dielectric loss factor of PPy was significantly high as compared to its composites with TGS; increased amounts of TGS in the composites resulted in less dielectric loss. In memory devices, materials with low dielectric loss factor are required to minimize the heat build-up within the device. Despite low dielectric permittivity, PPy/TGS composite can be effectively utilized as memory devices due to their low dielectric loss factor. Fig. 7d shows the variation in AC conductivity of PPy and PPy/TGS composites as a function of frequency. Variation in AC conductivity for PPy and the concerned composites was frequency independent.

5. Conclusions

PPy/TGS composites were successfully prepared by solution mixing method using DMF as solvent. TGA study revealed that decomposition of the composite was associated with a three- step degradation process. FESEM study showed the formation of nano-spherical structure for PPy, and the composite surfaces appear to be rougher than pure PPy. The DC conductivity of PPy was enhanced with increasing temperature, corroborating the excitation of electrons from the valance band to the conduction band. Reduction in DC conductivity of PPy/TGS composites compared to PPy was due to insulating behavior of TGS. Dielectric permittivity of PPy/TGS composites was found to be lower as compared to PPy. However, di-electric loss of the composite is substantially reduced, corroborating the application of the concerned composite as memory device.

Acknowledgments

This study was supported by the Converging Research Center Program (2011K000776), the Human Resource Training Project for Regional Innovation, and the World Class University (WCU) program (R31-20029) funded by the Ministry of Education, Science and Technology (MEST) and National Research Foundation (NRF) of Korea.

References

[1] N.T. Shanthi, P. Selvarajan, C.K. Mahadevan, Growth, structural, mechanical, spectral and dielectric characterization of NaCl-added triglycine sulfate single crystals, Curr. Appl. Phys. 9 (2009) 1155–1159.

[2] J.M. Chang, A.K. Batra, R.B. Lal, Growth and characterization of doped TGS crystals for infrared devices, Cryst. Growth Des. 2 (2002) 431–435.

[3] M.S. Pandian, N. Balamurugan, V. Ganesh, P.V. Rajashekar, K.K. Rao, P. Ramasamy, Growth of TGS single crystal by conventional and SR method and its analysis on the basis of mechanical, thermal, optical and etching studies, Mater. Lett. 62 (2008) 3830–3832.

[4] J. Novotny, J. Zelinka, F. Moravec, Broadband infrared detectors on the basis of PATGS/Pt(IV) single crystals, Sens. Acutat. A: Phys. 119 (2005) 300–304.

[5] C. Rai, K. Sreenivas, S.M. Dharmaprakash, Growth of 4-(dimethylamino) benzaldehyde doped triglycine sulphate single crystals and its characterization, Phys. B 404 (2009) 3886–3889.

[6] R. Muralidharan, R. Mohankumar, R. Dhanasekaran, A.K. Tirupathi, R. Jayavel, P. Ramasamy, Investigations on the electrical and mechanical properties of triglycine sulphate single crystals modified with some rare earth metal ions, Mater. Lett. 57 (2003) 3291–3295.

[7] R.B Lal, A.K. Batra, Growth and properties of triglycine sulfate (TGS) crystals: review, Ferroelectrics 142 (1993) 51–82.

[8] E. Venkatragavaraj, B. Satish, P.R. Vinod, M.S. Vijaya, Piezoelectric properties of ferroelectric PZT-polymer composites, J. Phys. D: Appl. Phys. 34 (2001) 487–492.

[9] T. Zhou, J.W. Zha, R.Y. Cui, B.H. Fan, J.K. Yuan, Z.M. Dang, Improving dielectric properties of $BaTiO_3$/ferroelectric polymer composites by employing surface hydroxylated $BaTiO_3$ nanoparticles, Appl. Mater. Interfaces 3 (2011) 2184–2188.

[10] Y. Yang, H.L.W. Chan, C.L. Choy, Properties of triglycine sulfate/poly(vinylidene fluoride-trifluoroethylene) 0-3 composites, J. Mater. Sci. 41 (2006) 251–258.

[11] J. Robertson, D.A. Hall, Nonlinear dielectric properties of particulate barium titanate-polymer composites, J. Phys. D: Appl. Phys. 41 (2008) 115407.

[12] H.C. Pant, M.K. Patra, Aditya Verma, S.R. Vadera, N. Kumar, Study of the dielectric properties of barium titanate-polymer composites, Acta Mater. 54 (2006) 3163–3169.

[13] S. Bose, N.H. Kim, T. Kuila, K.T. Lau, J.H. Lee, Electrochemical performance of a graphene-polypyrrole nanocomposite as a supercapacitor electrode, Nanotechnology 22 (2011) 295202.

[14] T.M. Wu, H.L. Chang, Y.W. Lin, Synthesis and characterization of conductive polypyrrole/multi-walled carbon nanotubes composites with improved solubility and conductivity, Compos. Sci. Technol. 69 (2009) 639–644.

[15] S. Bose, T. Kuila, M.E. Uddin, N.H. Kim, K.T. Lau, J.H. Lee, In situ synthesis and characterization of electrically conductive polypyrrole/graphene nanocomposites, Polymer 51 (2010) 5921–5928.

[16] T.M. Wu, S.H. Lin, Synthesis, characterization, and electrical properties of polypyrrole/multiwalled carbon nanotube composites, J. Polym. Sci. A 44 (2006) 6449–6457.

[17] Y. Wang, C. Yang, P. Liu, Acid blue AS doped polypyrrole (PPy/AS) nanomaterials with different morphologies as electrode materials for supercapacitors, Chem. Eng. J. 172 (2011) 1137–1144.

[18] M. Kotal, S.K. Srivastava, B. Paramanik, Enhancements in conductivity and thermal stabilities of polypyrrole polyurethane nanoblends, J. Phys. Chem. C 115 (2011) 1496–1505.

[19] M.G. Han, S.K. Cho, S.G. Oh, S.S. Im, Preparation and characterization of polyaniline nanoparticles synthesized from DBSA micellar solution, Synth. Met. 126 (2002) 53–60.

[20] A. Shakoor, T.Z. Rizvi, Synthesis and characterization of polypyrrole dodecylbenzenesulfonate-titanium dioxide nanocomposites, J. Appl. Polym. Sci. 117 (2010) 970–973.

[21] C. Basavaraja, N.R. Kim, E.A. Jo, R. Pierson, D.S. Huh, A. Venkataraman, Transport properties of polypyrrole films doped with sulphonic acids, Bull. Korean Chem. Soc. 30 (2009) 2701–2706.

[22] B.H. Kim, S.H. Hong, J. Joo, I.W. Park, A.J. Epstein, J.W. Kim, H.J. Choi, Electron spin resonance signal of nanocomposite of conducting polypyrrole with inorganic clay, J. Appl. Phys. 95 (2004) 1643198.

[23] P. Mavinakuli, S. Wei, Q. Wang, A.B. Karki, S. Dhage, Z. Wang, D.P. Young, Z. Guo, Polypyrrole/silicon carbide nanocomposites with tunable electrical conductivity, J. Phys. Chem. C 114 (2010) 3874–3882.

[24] S.A. Saafan, M.K. El-Nimr, E.H. El-Ghazzawy, Study of dielectric droperties of polypyrrole prepared using two different oxidizing agents, J. Appl. Polym. Sci. 99 (2006) 3370–3379.